Westerduinweg 3
1755 LE Petten
P.O. Box 15
1755 ZG Petten
The Netherlands

www.tno.nl

T +31 88 866 50 65

TNO report

TNO 2022 R10402

Energy management system for combined renewable generation, storage and conversion (EMERGE model): Renewable Hybrid Power Plant Optimization

Date	July 2022
Author(s)	Max Houwing, Nassir Cassamo, Edwin Wiggelinkhuizen
Copy no	
No. of copies	
Number of pages	35 (incl. appendices)
Number of appendices	1
Sponsor	
Project name	Energy management system for combined renewable generation and storage
Project number	060.47429

Summary

In order to accelerate the integration of renewable intermittent generation, such as wind and solar photovoltaics (PV), these assets can be combined in a Hybrid Power Plant (HPP) with energy storage, such as batteries, as well as conversion to different energy carriers, such as hydrogen and heat. Such an integration in an HPP can yield highly predictable generation, resulting in higher and more stable revenues, more flexible control that increase grid infrastructure utilization while reducing curtailment.

This work details the methodology to model such HPPs and optimize its operation to maximize the profit margin in different energy markets. The Energy Management systEm for combined Renewable Generation and storagE (EMERGE) model combines the main technical and economic aspects of an HPP into a single package, which allows for scheduling and planning of the HPP for the long and short term future, followed by simulation of the realized operation. The economic aspect of the EMERGE model uses optimization algorithms for the HPP assets to schedule their operation for the upcoming day, in the most profitable sense. The technical package within the EMERGE model then uses a representation of each HPP asset to simulate the actual day operation, identifying the resulting energy surplus and deficit of the plant. As shown at the end of this study, this combination of economical dispatch and the resulting technical analysis positions EMERGE to aid in preparation for small-scale testing in a lab setting and model validation, before full-scale implementation.

Contents

1 Introduction

Renewable technologies have been gaining momentum over the last decades, promising to help curbing the amount of greenhouse gas emissions. Such developments are incentivised by the European ambitions, with targets such as cutting carbon emissions by at least 55% by 2030 when compared with 1990 levels and making Europe climate neutral by 2050. Wind and solar photovoltaic (PV) power are currently two of the most widely used renewable technologies. However, as they are dependent on available resources (wind and irradiance), their power output will be intermittent, which is not desirable. An emerging trend in the energy industry is to combine multiple Distributed Energy Resources (DERs) with energy storage, such as batteries, as well as conversion to different energy carriers such as hydrogen and heat. Such a combination of assets is usually referred to as a Hybrid Power Plant (HPP) [1].

The tendency to combine assets in an HPP is motivated by the numerous advantages that can realized, such as increased Annual Energy Production (AEP) and capacity factor by storing excess energy instead of curtailing it. Furthermore, enhanced flexibility can be realized using an HPP, by making use of electricity arbitrage opportunities, using the batteries or hydrogen and heat conversion to access additional sources of revenue. Finally, the introduction of an HPP can reduce the impact of a lack of sufficient grid connection and transport capacity, as well as the power forecast error, making use of the energy storage and conversion to smooth the deviations between predicted and actual energy produced [2].

Different HPP configurations, EMSs, optimisation techniques and flexible control of power have all been studied in the literature [4, 5, 6]. For this optimization, minimization of the total levelized cost of energy during the expected lifespan of the HPP is a typical objective.

This work provides insights in the technical and economical aspects of an HPP, including asset utilization and energy flows, through development of the Energy Management systEm for combined Renewable Generation and storagE (EMERGE) model. For the economic aspects, the EMERGE model focuses on the economical dispatch of the assets in an HPP for the day ahead market. This optimization determines a schedule for the upcoming day that maximizes the revenue from renewable generation, stored energy or conversion of electricity, while minimizing the marginal cost of storage and conversion assets. For the technical aspects of an HPP, the EMERGE model uses static models of the HPP assets to simulate the actual operation of the HPP based on the schedule from the economical dispatch, and identifies the resulting surplus and deficit of the plant as a whole. This combination of economical dispatch and the resulting technical analysis enables EMERGE to be used in preparation for small-scale testing in a lab setting, before considering full-scale implementation.

This report is structured as follows: in Chapter 2, the modelling approach is detailed, introducing the structure of the developed EMERGE model, the assets it contains, and the optimization and cost modelling approach. Next, Chapter 3 discusses a case study to demonstrate the capabilities of the developed model.

2 Methodology

This chapter details the modelling approach of different components of TNO's Energy Management systEm for Renewable GeneratIon and storagE (EMERGE). This model is created to model the planning and operation of a Hybrid Power Plant (HPP) consisting of wind and solar PV generation, as well as battery storage, hydrogen conversion and heat production (Power2Heat). This chapter is structured in the following way: first, an overview of the model is shown in Section 2.1, followed by a description of the assets that are modelled in Section 2.2. Finally, an overview of the optimization and cost modelling approach is presented in Section 2.3.

2.1 Structure of the EMERGE model

The basic structure of the EMERGE model can be split in three parts: resource availability, optimization and simulation. A schematic overview of these three stages is shown in Figure 1 below.

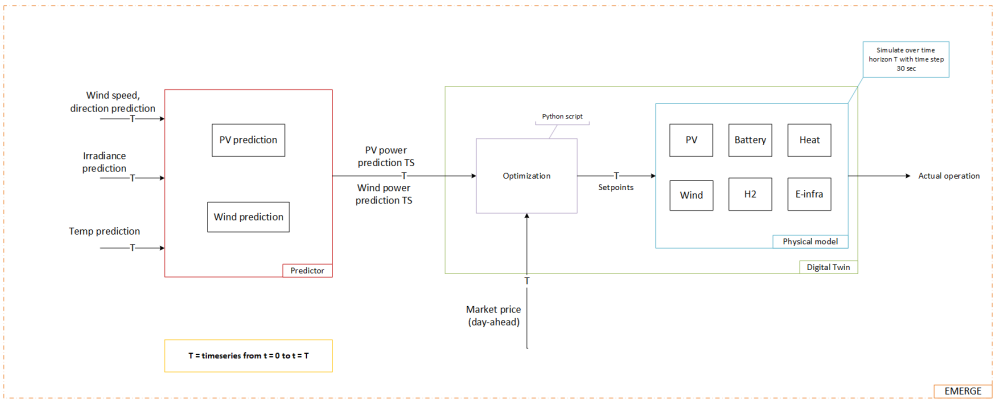

Figure 1: Schematic overview of the EMERGE process flow, with the different model steps highlighted.

First, the resource availability part of the model uses input of the atmospheric conditions for the day ahead, necessary to estimate the hourly power production of the wind and solar PV assets. This resource availability step, implemented in a Matlab/Simulink environment, makes use of a constant value of the atmospheric conditions for the complete hour, namely temperature, irradiation, wind speed and direction. These conditions are used to construct an hourly time series of expected production, which are then fed into the optimization stage.

The optimizer combines the time series of power prediction with the expected day-ahead market price, and uses profit optimization to determine set points for the generation, storage and conversion assets. These set points are normalized values between 0 and 1, which represent no or full generation/load for the respective asset. The exception to this is the battery system, which can accept a set point between -1 (full charge) and 1 (full discharge). The optimization is a Python-based mixed-integer linear programming (MILP) model, and includes simplified representations of the wind and solar PV generation, as well as the battery (storage), hydrogen and heat (conversion) assets. A more detailed description of the modelling approach for this optimization can be found in Section 2.3.1.

Finally, the set points determined by the optimization are fed into the physical model stage. This physical model uses MATLAB/Simulink to represent the operation during the day of the generation, storage and conversion assets. This operation is based on

a 30 second time step, and uses the set points that were determined in the optimizer for the day ahead. The assets modelled in this stage are described in more detail in Section 2.2.

2.2 Overview of assets modelled in the EMERGE model

This section presents an overview of the assets modelled in the EMERGE tool. First, the wind and solar PV generation assets are detailed in Section 2.2.1 and 2.2.2, respectively. Next, the battery storage is described in Section 2.2.3, followed by the hydrogen conversion in Section 2.2.4. Finally, the heat conversion asset is described in Section 2.2.5.

2.2.1 Wind Farm

The wind farm model used in the EMERGE tool is based on the FLORIS wind farm model [9]. The simplicity and fast calculation speed makes this model very suitable for use in these optimization algorithms. Finally, the wind farm has been extended here to allow for regulation of the wind turbine output power based on the set point coming from the optimizer.

2.2.2 Solar PV

The solar PV farm is constructed based on individual solar PV panels, which are modelled as an equivalent circuit [10, 11, 12]. This model uses the irradiance, ambient temperature and panel specific inputs, such as the energy band gap and open circuit voltage, to calculate the PV panel power production. Because of the dependence on panel specific inputs, the model can easily be configured for different PV panels. Additionally, it is possible to configure the undersizing of the PV plant inverters, a common trade-off between energy yield maximisation and inverter cost minimisation, and the PV plant efficiency. This efficiency governs the conversion from a single panel to a full-scale PV plant, accounting for losses such as cabling or shading effects. Similar to the wind farm, regulation of the PV plant output power is available, based on the set point from the optimizer.

2.2.3 Battery energy storage system (BESS)

The battery system is modelled as an equivalent circuit cell, as typically done in literature [13]. This model uses battery specific data such as the battery constant voltage, rated capacity and polarisation voltage to calculate the current capacity, based on the instantaneous current and voltage. In addition, a battery management system (BMS) is modelled that governs the behaviour of the battery in response to a set point, limiting the upper and lower state-of-charge (SOC) and (dis)charging current of the system. Additionally, the battery system model can emulate reduced charging rates above a certain threshold, as is commonly seen in Lithium-ion chemistries, as well as reduced discharge rates below a certain threshold, which is common due to decreasing voltages at low SOC.

2.2.4 Hydrogen conversion asset

The electrolyser used for hydrogen conversion is modelled as a status-based static model, using different look-up tables for the different operational states [14], [15]. Furthermore, the stack and balance of plant (BOP) power consumption, ramp rates and operational mode switching time, e.g. from standby to full production, are considered when following the incoming set point. The model is able to represent several typical operational states, such as the full shutdown state, cold/hot standby and fully operational state. The switching between these states occurs based on the (lack of) incoming set point. When the electrolyser is in a state other than the full operational

state, the hydrogen production (in kg/s) will be limited due to electrochemical, thermal and pressure limitations from the electrolyser (re)starting.

2.2.5 Heat conversion asset

For the heat conversion asset, a heat pump is modelled based on typical thermodynamic relations [16]. This model relates the power flowing into the heat pump to the heat output of the asset, using the coefficient of performance (COP). This COP depends on the ambient and desired temperature, as well as a performance indicator of the heat pump itself. Finally, the heat pump can follow a set point between the minimum and maximum operating (input) power.

2.3 Economic optimisation and cost modelling within the EMERGE model

2.3.1 Optimising for day ahead profit

In this section, the profit optimization mechanism is specified using the equations of the mixed-integer linear programming (MILP) problem. The objective of this profit optimization is to maximize the profit C_t^{pr} (in €) for the set of timesteps t, as specified in Equation 2.1.

maximize:

$$\sum_t C_t^{pr} = \sum_t [C_t^{rev} - C_t^c] \tag{2.1}$$

In this objective function, the revenue C_t^{rev} and cost C_t^c (in €) are calculated from Equation 2.2 and 2.3, respectively.

$$C_t^{rev} = [P_t^{exp} \cdot \lambda_t^{el} + P_t^{H2} \cdot \lambda_t^{H2} + P_t^{heat} \cdot \lambda_t^{heat}] \cdot \Delta T \tag{2.2}$$

$$C_t^c = [P_t^{imp} \cdot \lambda_t^{el} + (P_t^{bat,in} + P_t^{bat,out}) \cdot C_t^{m,bat} + P_t^{H2} \cdot C^{m,H2} + P_t^{heat} \cdot C^{m,heat}] \cdot \Delta T \tag{2.3}$$

where P_t^{exp} is the exported power (in W), ΔT is the timestep (in seconds), λ_t^{el} is the day-ahead price (in €/Wh), P_t^{H2} is the power input to the electrolyzer (in W), λ_t^{H2} is the hydrogen price (in €/Wh), P_t^{heat} is the power input to the heat pump (in W), λ_t^{heat} is the heat price (in €/Wh), P_t^{imp} is the imported power (in W), $P_t^{bat,in}$ and $P_t^{bat,out}$ are the battery charging and discharging power (in W), respectively, and $C_t^{m,bat}$, $C^{m,H2}$ and $C^{m,heat}$ are the battery, hydrogen and heat cost, respectively (in €/Wh).

The marginal battery cost $C_t^{m,bat}$ is assumed to vary depending on the relative battery load, as elaborated on in section 2.3.2.

The model needs to ensure the incoming power from generation, storage and import is equal to the outgoing power to export, storage, hydrogen or heat production. This balance is described in Equation 2.4.

$$P_t^{wind} + P_t^{PV} + P_t^{bat,out} + P_t^{imp} = P_t^{exp} + P_t^{bat,in} + P_t^{H2} + P_t^{heat} \tag{2.4}$$

In this equation, the output wind power P_t^{wind} (in W) is determined by the wind setpoint sp_t^{wind}, the predicted normalized wind power $P_t^{w,pred}$ and rated wind power P^{wind} (in W), as defined in Equation 2.5.

$$P_t^{wind} = sp_t^{wind} \cdot P_t^{w,pred} \cdot P^{wind} \tag{2.5}$$

Similarly, the PV power P_t^{PV} (in W) is determined from the PV setpoint sp_t^{PV}, predicted normalized PV power $P_t^{PV,pred}$ and maximum PV power P^{PV} (in W), as defined in Equation 2.6.

$$P_t^{PV} = sp_t^{PV} \cdot P_t^{PV,pred} \cdot P^{PV} \tag{2.6}$$

Finally, the hydrogen and heat input power is determined using Equation 2.7 and 2.8, respectively, where sp_t^{H2} and sp_t^{heat} are the respective setpoints, and P^{H2} and P^{heat} the rated power (in W).

$$P_t^{H2} = sp_t^{H2} \cdot P^{H2} \tag{2.7}$$

$$P_t^{heat} = sp_t^{heat} \cdot P^{heat} \tag{2.8}$$

The charging and discharging of the battery is limited by the Equation 2.9 and 2.10, respectively. These equations ensure that the bi-directional power flow in and out of the battery can never exceed the maximum power available, defined by $P^{b,ch,max}$ and $P^{b,dis,max}$ (in W), multiplied by the setpoints $sp_t^{b,in}$ and $sp_t^{b,out}$ and efficiency η_{bat} to obtain the actual power of the battery.

$$P_t^{bat,in} \leq sp_t^{b,in} \cdot \eta_{bat} \cdot P^{b,ch,max} \tag{2.9}$$

$$P_t^{bat,out} \leq sp_t^{b,out} \cdot \eta_{bat} \cdot P^{b,dis,max} \tag{2.10}$$

Equation 2.11 and 2.12 are binary constraints, added to ensure the battery can only be charging or discharging at any given time, and not both. These are specified as a Big-M constraint [17], where M_{bat} is a very large number, and u_{bat} is a binary variable.

$$P_t^{bat,in} \leq M_{bat} \cdot u_{bat} \tag{2.11}$$

$$P_t^{bat,out} \leq M_{bat} \cdot (1 - u_{bat}) \tag{2.12}$$

Similar to the battery binary constraints, Equation 2.13 and 2.14 define binary constraints for import and export of power, again using a Big-M constraint where M_{exp} is a very large number, and u_{exp} is a binary variable.

$$P_t^{imp} \leq M_{exp} \cdot u_{exp} \tag{2.13}$$

$$P_t^{exp} \leq M_{exp} \cdot (1 - u_{exp}) \tag{2.14}$$

The battery state-of-charge SOC_t^{bat} is initially defined by Equation 2.15, and calculated for every subsequent timestep using Equation 2.16. Here, the new SOC is determined

from the previous SOC, to which the charged energy is added and from which the discharging energy is subtracted. Here, $E^{b,cap}$ is the rated battery capacity (in Wh).

$$SOC_t^{bat} = SOC^{b,init}, t = 0 \tag{2.15}$$

$$SOC_t^{bat} = SOC_{t-1}^{bat} + [P_t^{bat,in} - P_t^{bat,out}] \cdot \Delta T \tag{2.16}$$

2.3.2 *Cost modelling of assets*

The marginal battery cost $C_t^{m,bat}$, as defined in Equation 2.3, is assumed to vary depending on the battery load, as defined in Equation 2.17. This relation is based on literature [18] and approximates the degradation of the battery due to load, as shown graphically in Figure 2. This degradation is assumed to be at its minimum, per kWh (dis)charged, for approximately half load or $P_t^{b,rel} \approx 55\%$, with the relative battery usage $P_t^{b,rel}$ defined in Equation 2.18.

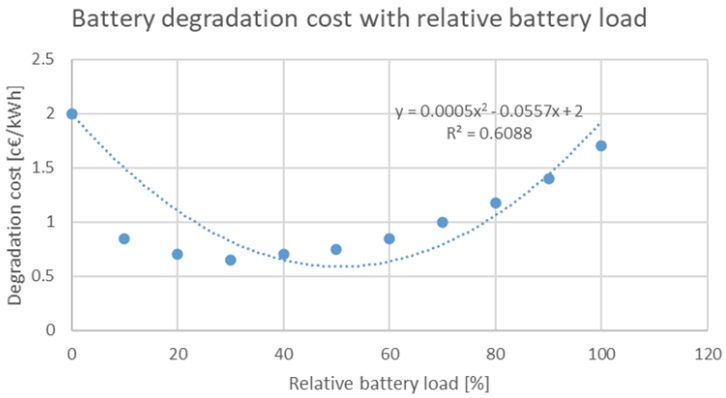

Figure 2: Approximation of battery degradation, in c€/kWh, due to relative battery usage. Adapted from [18].

$$C_t^{m,bat} = \frac{5 \cdot 10^{-4} \cdot (P_t^{b,rel})^2 - 5.57 \cdot 10^{-2} \cdot P_t^{b,rel} + 2}{100} \tag{2.17}$$

$$P_t^{b,rel} = (\frac{P_t^{bat,in}}{P^{b,ch,max}} + \frac{P_t^{bat,out}}{P^{b,dis,max}}) \cdot 100 \tag{2.18}$$

The optimization algorithm of the EMERGE tool takes into account the hydrogen production costs and revenues in order to maximize the profit for the system. This is done depending on the specified time horizon, defining the set-points for this horizon assuming a perfect prediction of electricity prices and solar and wind resources. Electricity will flow to the electrolyser either from the market, the PV plant, the wind power plant or the battery depending on the profit maximization of the overall plant.

The costs and revenues are therefore necessary for each time step. The costs of the produced hydrogen are expressed in €/kgH2 produced. These costs are based on reports which indicate the potential cost for green hydrogen production from PEM electrolysis. The cost of hydrogen coming from electricity sources (wind and solar) would ideally be tied to their subsequent costs. Therefore, a fully renewable based electricity market clearing price would be an indicator of the expected hydrogen cost, but for the case here, a constant value is assumed as a simplification [19], [20].

3 Exemplifying case study

This section details an exemplifying case study used to demonstrate the capabilities of the EMERGE model. As an illustration of the functionalities of EMERGE, this case study is not intended as a realistic measure of its performance. The section is structured in the following way; first, the input data used for the case study is described in Section 3.1. Next, the calculation of the available wind and solar generation for the day ahead is detailed in Section 3.2. Finally, the results of the optimization and subsequent simulations of asset models are presented in Section 3.3.

3.1 Hybrid power plant asset input data

3.1.1 Wind farm approach and inputs

The available wind power is calculated using the FLORIS wake model, described in Section A.1. The wind resource availability is simulated using 1 minute measurements from a meteorological mast. This mast is located in nearby the village Wieringermeer in the Netherlands, where the terrain is flat and nearby the large IJsselmeer lake. The data has been recorded on September 9, 2014, with a daily average wind velocity of 8 m/s and wind direction of 250°, approximately. A turbulence intensity of 14% is assumed in the simulations (not present in the data). For such wind directions, the mast is located in free stream conditions with respect to surrounding wind turbines.

With a lack of additional data available, the same wind data has been used for both day ahead prediction, and actual day simulation. Ideally, hind-cast weather forecast and actual weather measurements would be used, if available. To avoid using completely identical data for this case, the day-ahead prediction only uses the hourly averages of the wind velocities and directions, as required for the day-ahead optimization. This does result in some wind inflow variability in the simulations performed to evaluate the outcome of the optimized management strategy as compared to the simulations used in the optimization itself. More realistic scenarios will be considered in the future including proper modelling of the uncertainty inherent with the prediction of the wind conditions.

3.1.2 Solar farm approach and inputs

The available solar power is calculated using the static solar panel model based on the analytical P-V curves, as described in section A.2. To simulate the model, 3 different inputs are needed: the irradiance, temperature and wind. The irradiance and temperature directly dictate the shape of the P-V. The temperature is influenced by both the irradiance, ambient temperature and wind speed, as equation A.5 in Section A.2 specifies.

The irradiance and ambient temperature data is taken from the Measurement and Instrumentation Data Center (MIDC) [21], from the National Renewable Energy Laboratory (NREL) which provides irradiance and meteorological data from stations around the United States of America.

These data was used as it was found to be one of the few sources available online for high frequency time series, i.e., data at each 60 seconds time step. It is often the case that solar irradiance data available online is at lower frequencies (5 minute or hourly based). Given that the goal of the EMS is to simulate at each 30 seconds, it is believed that this dataset provides a good starting point for initial simulations for the purposes of testing.

For the specific case which constitutes the bulk of section 3, data from Oak Ridge National Laboratory (RSR) [21] is used. The data spans from the 1st of January 2018 to the 1st oF December 2019, enabling the user to perform sensitivity studies on the results of different weather conditions.

3.1.3 Optimisation case study inputs

The prices used for this case study are depicted in Figure 3. The shape of the electricity prices curve is a typical one during a weekday, with peaks in the morning and evening. For this study, it has been assumed that the price to buy energy is the same as the price to sell energy.

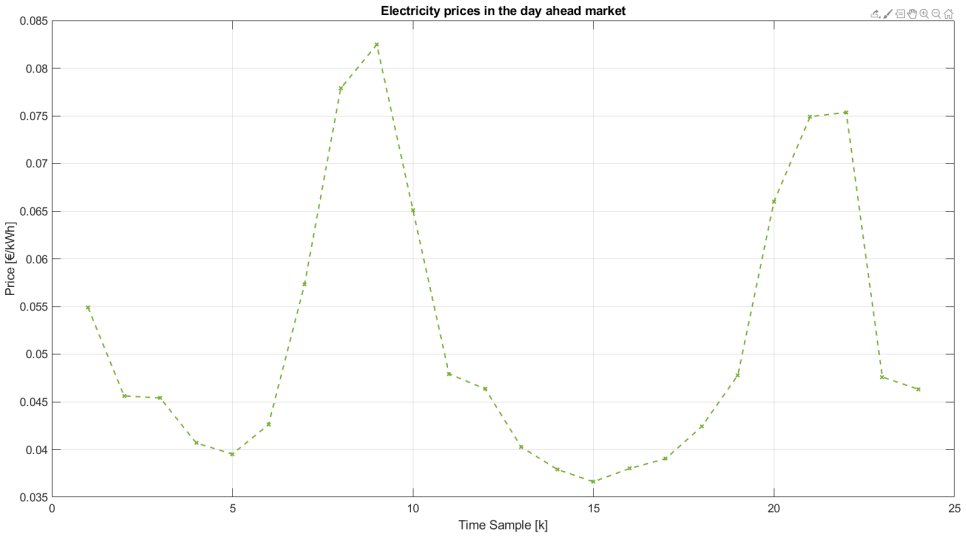

Figure 3: Day ahead electricity prices used for the optimisation.

The study is conducted over 1 day, with time steps of 1 hour each. In practical terms, 24 setpoints are defined so that the assets dispatching will occur at each hour. The assets are chosen to have the following rated power/capacity:

- Wind Farm: 60 kW
- Solar Farm: 40 kWp
- Battery (capacity): 50 kWh
- Electrolyser: 25 kW
- Heat Pump: 10 kW

Furthermore, the HPP is restricted from importing and exporting a certain amount of power at each time instant. For this specific study, the HPP is limited to buying a maximum 11 kW and selling at most 11 kW, to emulate severely restricted grid infrastructure. In addition, the battery is set to be at a SOC of 0.5 at the beginning, with the charging and discharging power set to 0.5C, or 25 kW. The battery efficiency is assumed to be 95% (one way). The heat pump COP is assumed to be 5 and the total heat to be delivered is set to $3 \cdot 10^5$ Wh_e. In terms of costs and prices, the values used are €0.1/kWh for the hydrogen revenue, and €0.05/kWh for production cost. This translates to roughly €5/kg and €2.5/kg, depending on the assumed efficiency.

3.2 Calculating total day ahead energy production

The first step in the EMERGE model is to make use of the weather forecast values to simulate the expected energy production during in the day ahead. This allows to bid a certain amount of energy on the day ahead market. The scope of this work does not involve developing forecasting models. The literature is vast in that area and in practical terms, it may be more logical to simply resort to other parties who are experts in providing such forecast, such as weather forecasting companies. Therefore, the goal here is to make use of known measurements (the data that has been described in subsection 3.1).

The inputs for the wind and solar models can be seen in detail in Figures 4 and 5, corresponding to the Wind Farm and Solar Farm variables, respectively. In these figures, only the data for the first day used for the simulation is shown.

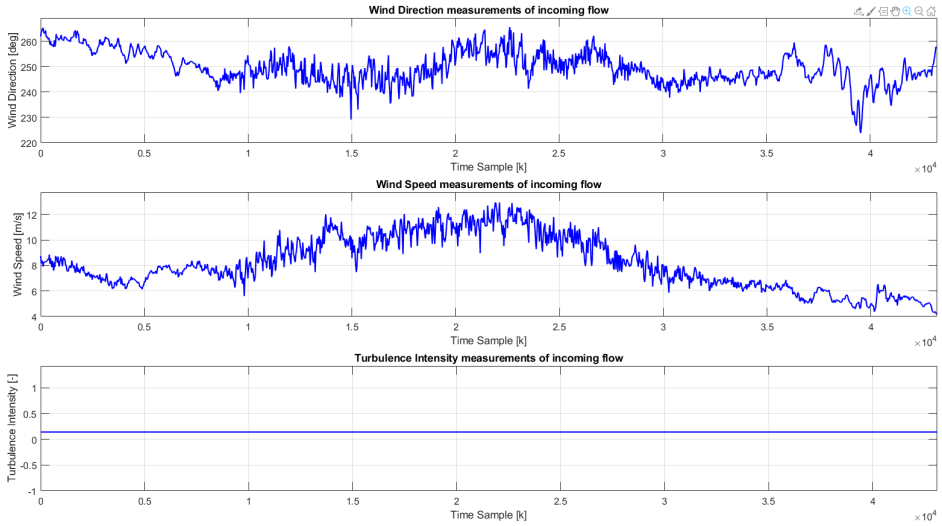

Figure 4: Wind Farm input measurement used for the purposes of simulation.

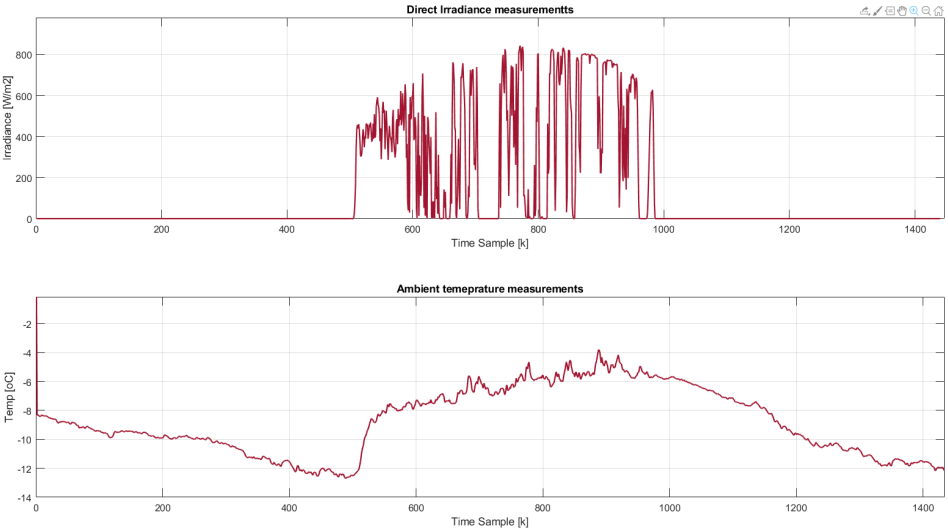

Figure 5: Direct irradiance and ambient temperature measurements used for the purposes of simulation.

Figures 6 and 7 show the scopes of the models available in EMERGE during simulation. The Wind Farm model shows the different variables for each of the turbines available

in the wind farm. Different lines of different values are visible, as each one corresponds to one turbine that will register a different value. The first plot depicts wind speed turbine measurements which differ due to wake effects within the farm. The second represents the total produced power of the farm (by summing the power produced at each turbine). The third and fourth plots show the control variables of each wind turbine, specifically the blade pitch angle and the generator torque.

The PV panel overview shows the input irradiance data in the first plot. The second plot contains the ambient temperature and the solar module temperature. The final plot is the power output of each PV panel array. Note that the increase in internal temperature of the PV panels is unintended behaviour caused by negative irradiance from the input data, which will be fixed for future cases. For this simulation 4 distinct lines are seen, that corresponds to the 4 solar arrays used for this simulation. Two of them have a rated power of 13kW and the other 2 a rated power of 6.5Kw, giving a total rated power of the solar farm of 40kW.

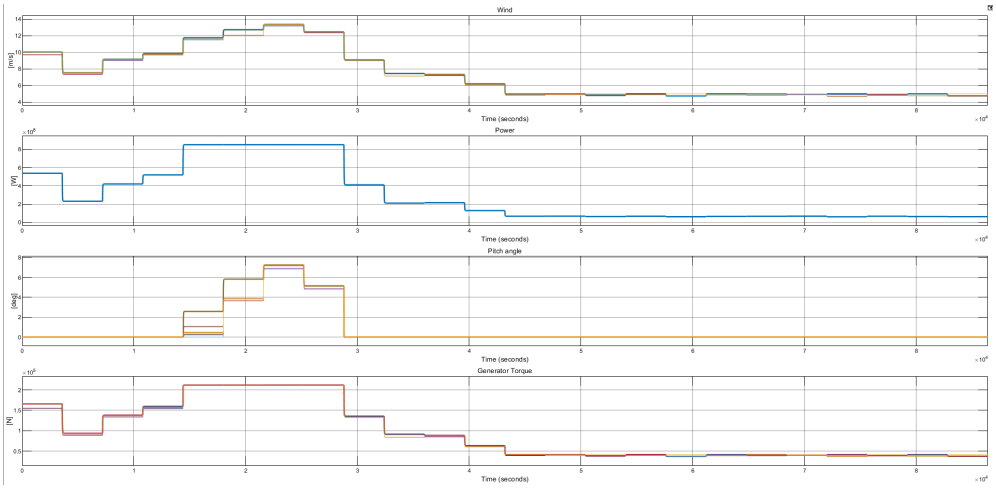

Figure 6: Wind Farm variables during simulation for computation of available power at each hour in the day ahead.

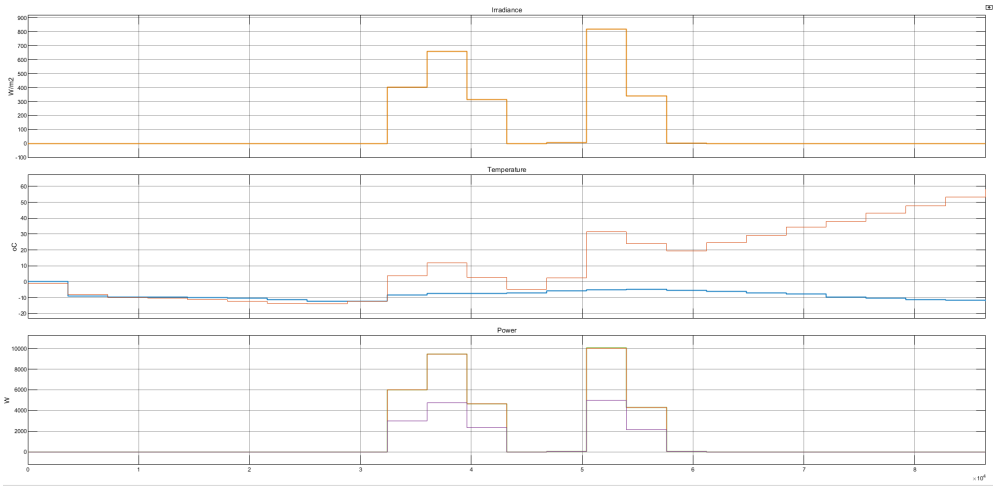

Figure 7: Solar Farm available variables throughout simulation for computation of available power at each hour in the day ahead.

The EMS in this work was designed with the goal of becoming a versatile and flexible tool which could be used for different purposes. Although the wind farm model and solar farm model have different sizes and power production with different orders of magnitude, all this power is normalized to the rated power of each asset. This means

that the final power production forecast for the day ahead will be normalized, becoming a time series whose values are lower than one.

The next step is to take into account this normalised power forecast for the optimisation step. The available power profile and day ahead market prices, which are assumed to be known, are used in the optimization step described in Section 3.3 to optimise the day ahead set points to dispatch the several assets, with the final aim of maximising the cumulative profit.

3.3 Optimisation and asset model results

The second step is to optimise the day ahead hourly dispatching of assets, based on the input data described in Section 3.1.3. For this, each asset operational set point, a value between 0 and 1 which dictates at what percentage of the rated power the asset should be functioning, is calculated. The set points are computed by solving an optimisation problem where the profit is maximised. The revenue originates from the sale of hydrogen and electricity, while the cost comes from the production of electricity and marginal cost of the storage and conversion assets.

Given the defined values, the input/output information is evaluated. The input information are the depicted day ahead prices, and the hourly power forecast detailed in subsection 3.2, both of which are then normalized. The final input information is condensed in Figure 8.

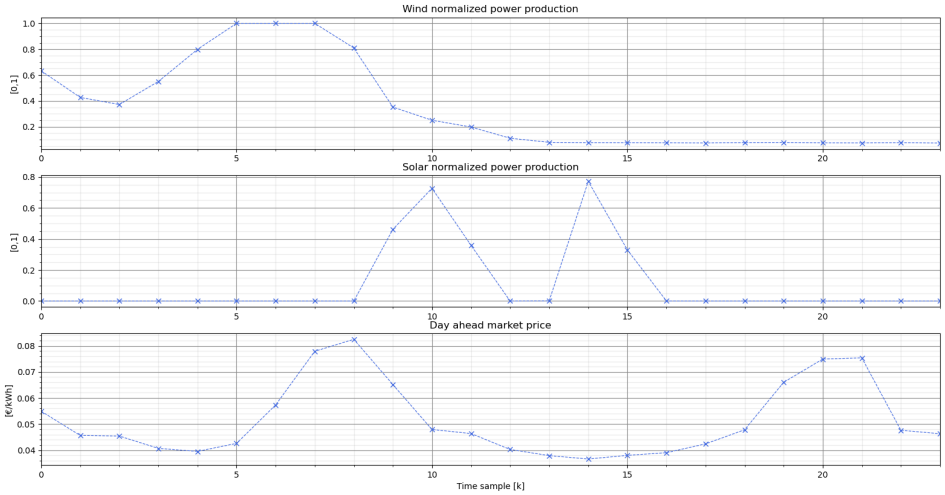

Figure 8: Optimiser inputs: normalized power production from generating sources (wind and solar) and day ahead energy market prices

The output of the optimiser is depicted below, in Figures 9, 10 and 11. From Figure 9 some patterns of interest are already visible.

The first is during the first part of the day, where it can be seen that the availability of resources is used to charge the battery and produce hydrogen. Additionally, some curtailment is visible, due to all assets being dispatched (battery storing energy, hydrogen and heat producing) and the export cable is also at its maximum capacity, so the generating assets should reduce energy production.

The second example is towards the evening (after time sample 15). It can be seen that the wind and solar resources are being fully dispatched with a set point equal to 1. Nevertheless, the normalized wind and solar production is at its minimum at this time instant.

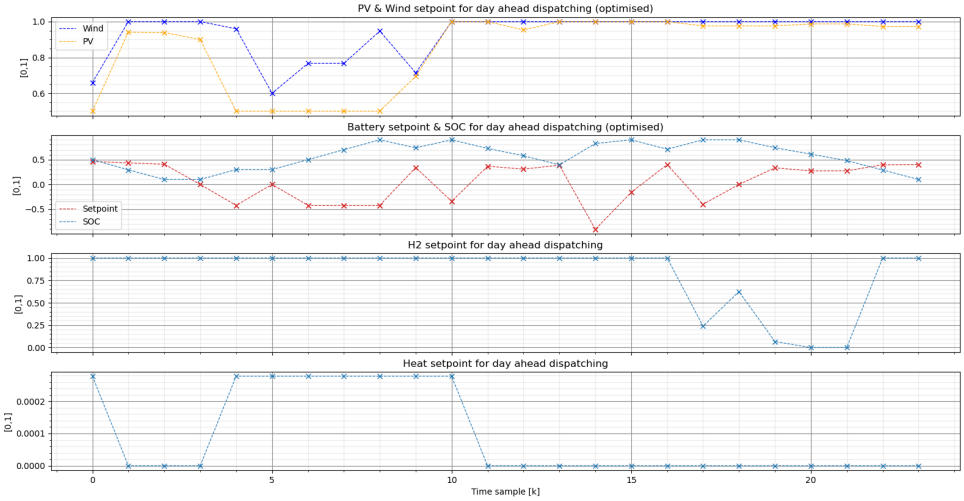

Figure 9: Day ahead set points for power dispatching. The first plot contains the set points for the generating assets and the remaining plots show the set points for the flexible assets: battery, electrolyser and heat pump.

Figure 10 shows the relation between battery usage and cost of operating the battery. As it was previously shown, the battery cost is tied with its operation. As described in Section 2.3.2, during periods of time when the battery is not being used the cost is the highest and when its being fully utilised the cost is lowest.

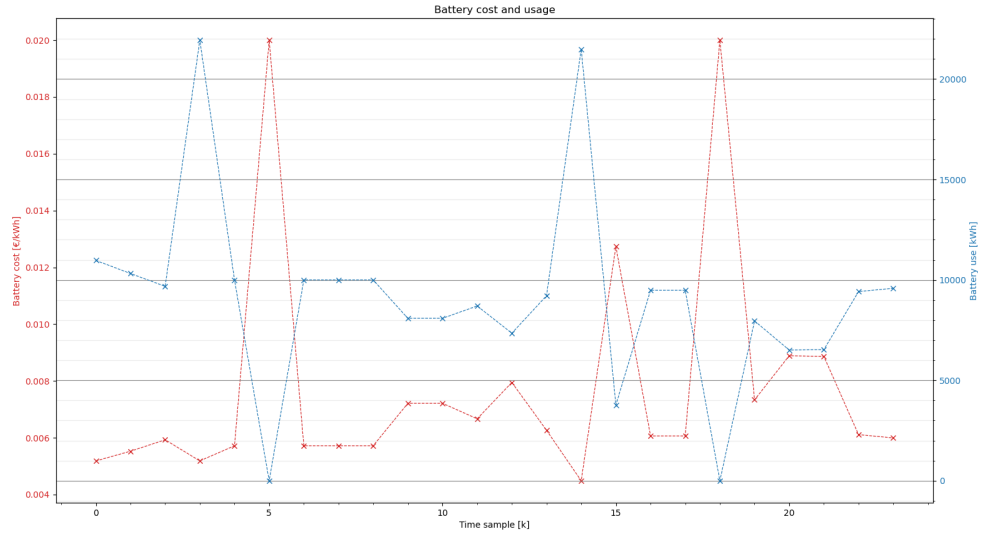

Figure 10: Comparison between cost incurred by operating the battery and battery usage.

Finally, the model can produce an overview of the overall expected profit, as shown in Figure 11. It should be noted that there appears to be an instant where the profit is negative, which can be explained by simultaneous import of power and the fact that the battery is at its highest operating cost.

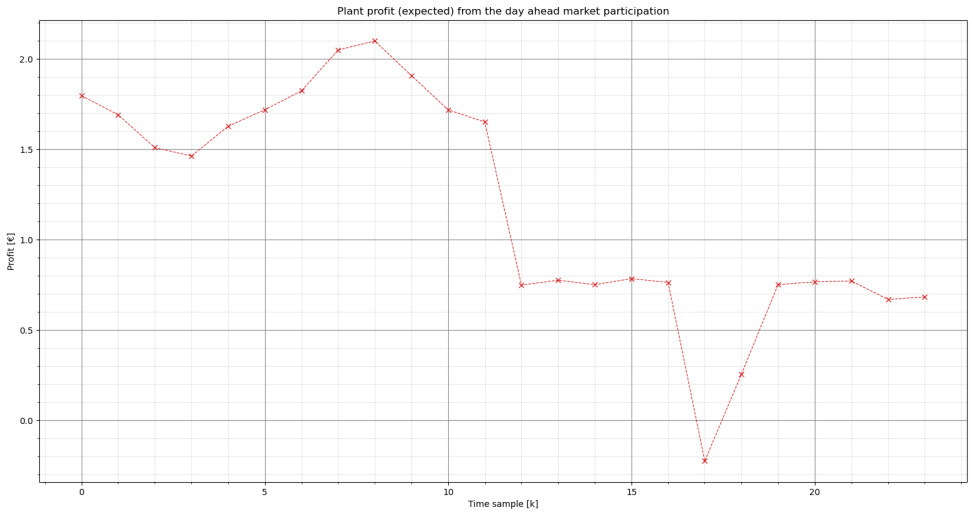

Figure 11: Total expected profit for HyPP operation in the day ahead market.

3.3.1 Simulating the Hybrid Power Plant

The final stage consists in simulating the Hybrid Power Plant based on the setpoints computed by the optimiser. This simulation is run with a timestep of 30 seconds. The final model to be simulated, in its full, is illustrated in Figure 12.

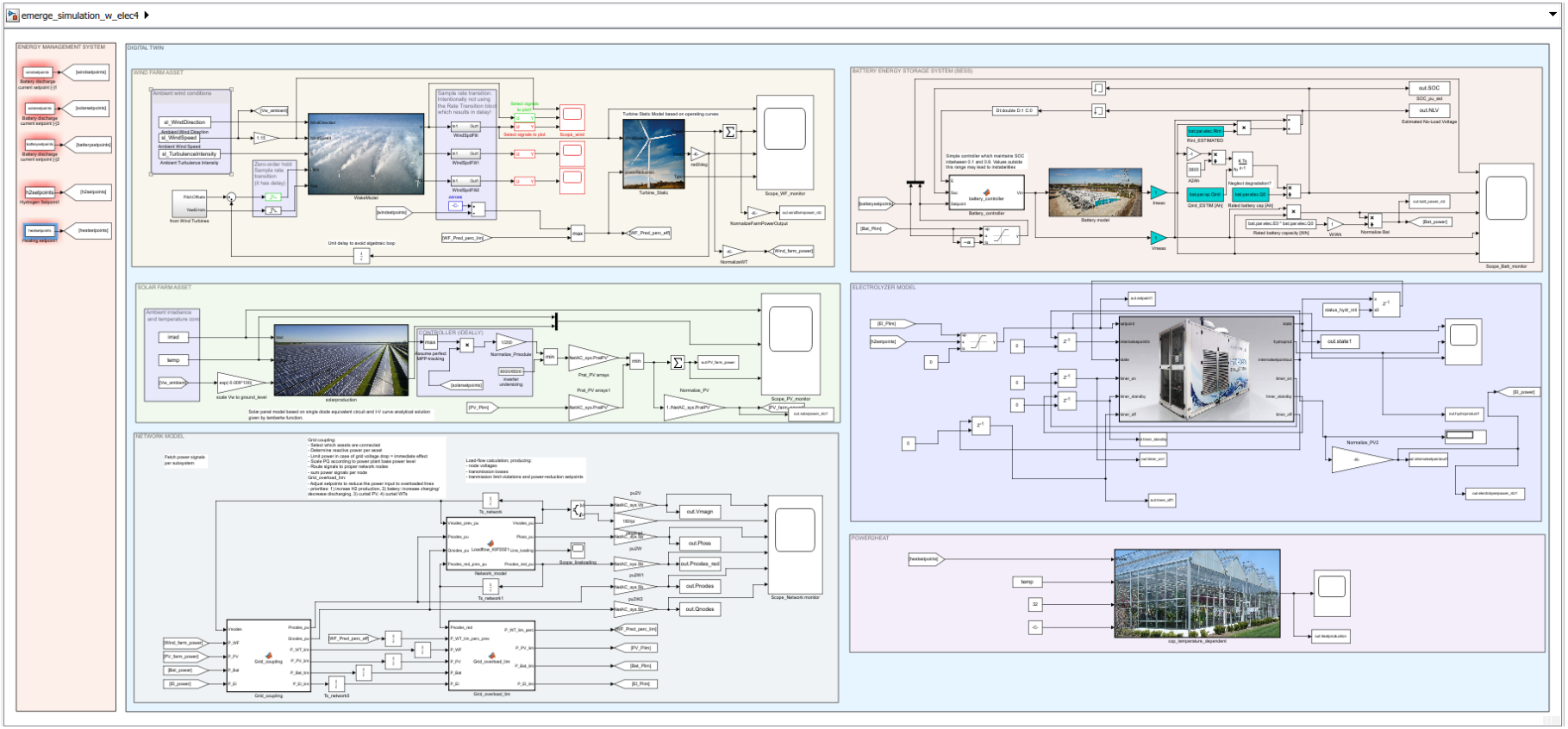

Figure 12: Hybrid Power Plant static model implemented in Simulink. On the left, the set points computed by the optimiser, with a predefined time advance (for this simulation, they are valid for 1 hour). In the middle, the different models representing the energy producing assets and the flexible assets.

In Section 3.3.1.1, 3.3.1.2 and 3.3.1.3, the results of a day simulation are shown and the behaviour of the models is shown.

3.3.1.1 Generating assets: wind farm and solar farm

For the wind farm plant, the control variables are shown for a timestep of 30 seconds for all turbines in the wind farm. This is visible in the scope presented in Figure 13.

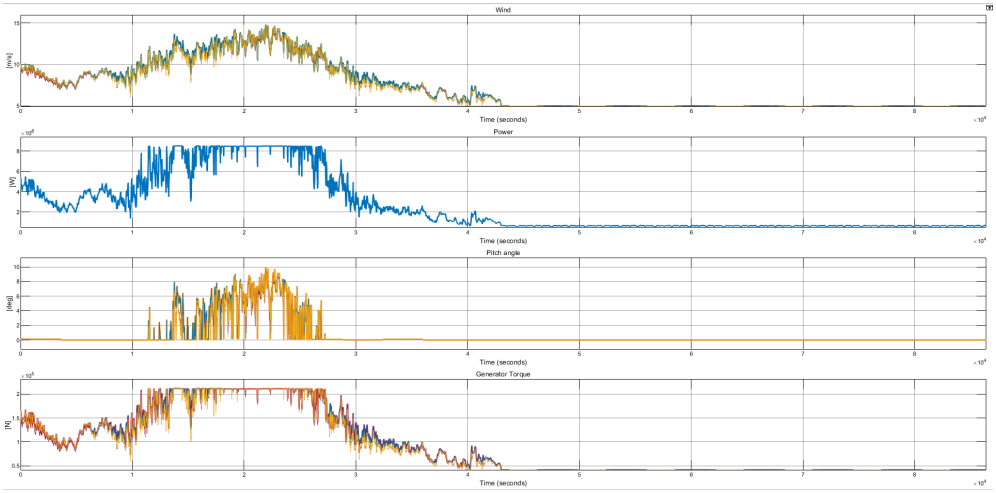

Figure 13: Wind Farm model scope. Channels presented, from first to last: wind turbine measured wind, power, blade pitch angle and generator torque. Full simulation of 1 day advancing at each 30 seconds.

The solar PV scope for the day simulation is presented in Figure 14, with irradiance data available for each 30 seconds. Again, note the internal temperature rising constantly when irradiance is supposed to be zero, which will be corrected for future cases.

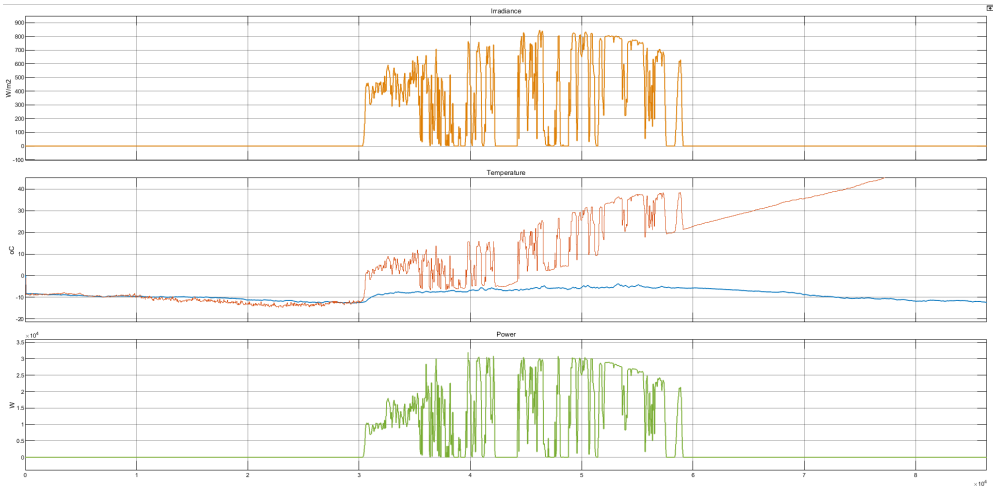

Figure 14: Solar Farm model scope. Channels presented, from first to last: Direct irradiance, temperature and output power. Full simulation of 1 day advancing at each 30 seconds.

3.3.1.2 Flexibility assets: battery, electrolyser and heat pump

The battery behaviour is represented in Figure 15. Note that despite the setpoints changing for a certain desired value, the battery, requires more time to charge or discharge due to its physical limitations. Furthermore, the limitation of the SoC between 0.1 and 0.9 is ensured by the battery management system.

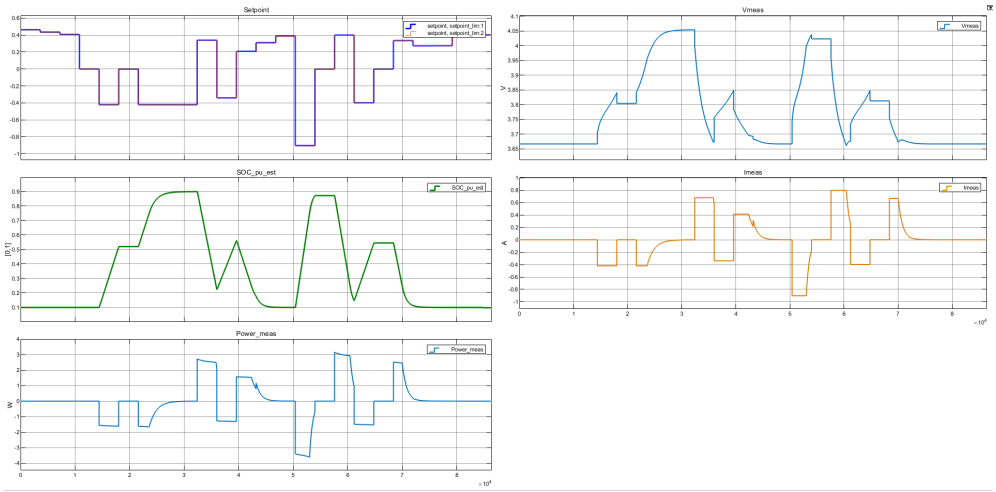

Figure 15: Battery model scope. Channels presented, from left to right, top to bottom: commanded set point, State of Charge [SoC], measured power, measured voltage and measured current.

The electrolyser behaviour is shown in Figure 16. Note that for this case, the operational status of the electrolyser is maintained at all times in its operation state (state 2). This is caused by the setpoint for hydrogen production being maintained at 1 for the majority of the time, so the electrolyser never enters standby (state 1).

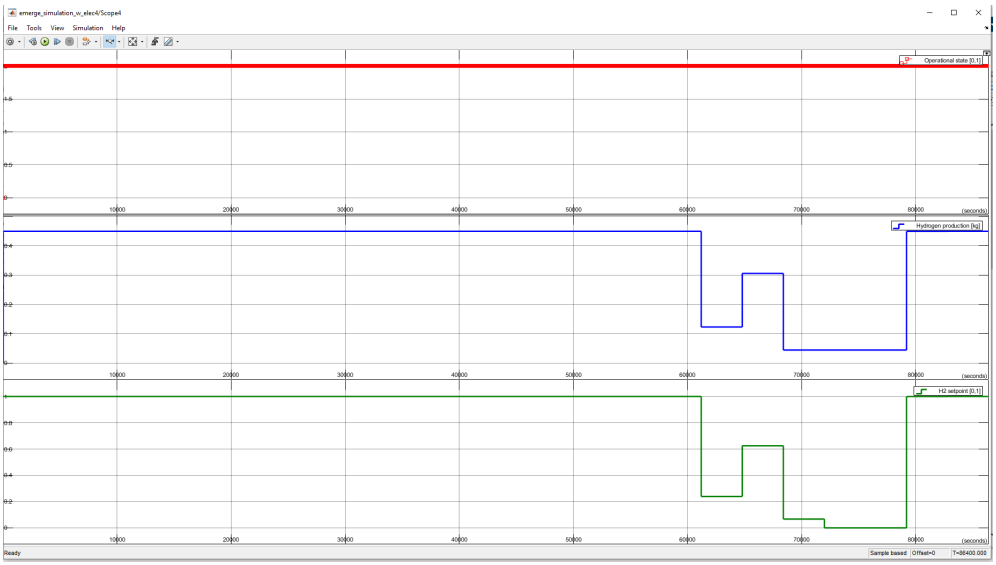

Figure 16: Electrolyser model scope, showing the operational state (top), hydrogen production (middle) and set point (bottom).

The heat pump power production (normalized) is shown in Figure 17. Note that the air temperature is taken as a varying argument and the internal desired temperature is 32 degrees Celsius.

3.3.1.3 Electrical network

The configuration of the assumed local (3-phase 50Hz. AC) electrical network for this case study is described in Table 1. In this case, Node 1 is connected to the public grid, which is configured as a slack node with a voltage set to 400V. As example of how to read this table, the maximum power supplied to node 7, supplied by WT6 and PV4, is equal to 16.5kW. Furthermore, the power supplied to node 10 can vary between 50kW

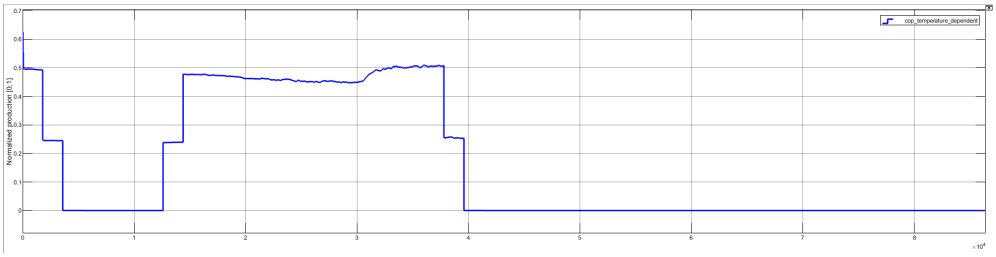

Figure 17: Heat pump model scope, showing the normalized heat production.

(with the battery discharging at 50kW) and -74kW (with the battery charging and the electrolyzer in full production)

Table 1: Electrical network configuration

Asset	Node	Rated power
WT_1 [V]	2	10kW
WT_2 [V]	3	10kW
WT_3 [V]	4	10kW
WT_4 [V]	5	10kW
WT_5 [V]	6	10kW
WT_6 [V]	7	10kW (2x6kVA inverter)
PV1 [V]	8	13kWp (2x6kVA inverter)
PV2 [V]	9	13kWp (2x6kVA inverter)
PV3 [V]	6	6.5kWp (6kVA inverter)
PV4 [V]	7	6.5kWp (6kVA inverter)
Battery [V]	10	50kW
Electrolyzer [V]	10	24kW

An example output of the electrical network behavior is depicted in Figure 18.

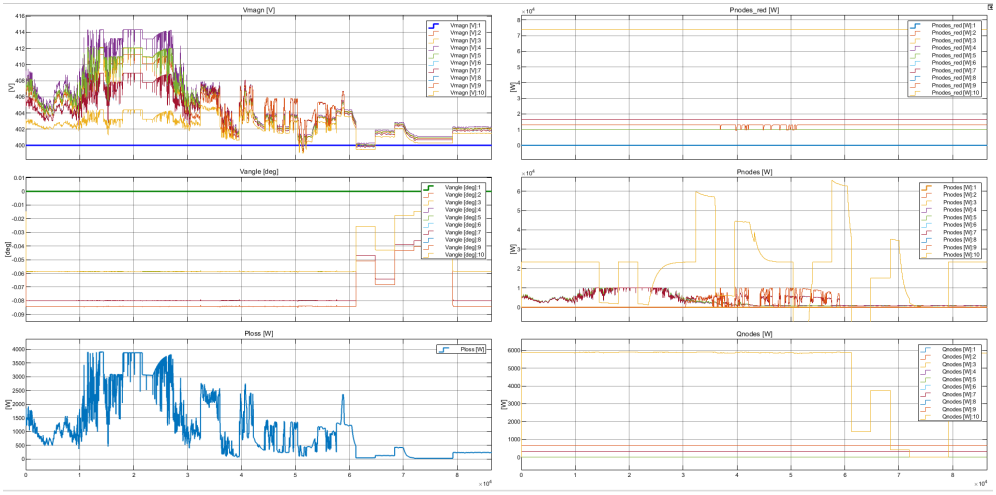

Figure 18

The left side (from top to bottom) shows:

1. The magnitude of the voltages at all nodes of the local network. Node 1, which is the connection to the public grid, is a slack bus with the voltage set to 400V. The other bus voltages rise with the power supplied to the grid bus.
2. The phase angle differences of the node voltages, relative to the zero-angle of node 1, are practically zero as the network is very small with a mainly resistive impedance.

3. The total power losses in the local network.

The right side (from top to bottom) shows:

1. The limits set to the power flow per node. In case of an oversupply, such that a line in the network would be overloaded, the model sets limits to the supply or demand of one or more nodes in order to resolve the overloading.
2. The supplied (+) or consumed (-) active power per node
3. The supplied (+) or consumed (-) reactive power per node. Note that the reactive power settings of the individual assets are for the moment implemented as fixed, user-set, reactive power levels or power factors.

The final results of the case study can be summarised in just one dashboard, which shows a comparison between optimized and realized operation, as well as energy flows. In particular, for each asset an overview is shown of the set point, energy, and difference in optimized and realized energy (delta), with the battery asset also showing the expected and realized state-of-charge (SOC). In addition, the market prices with the relevant profit margins for the flexibility assets are shown, as a total realized revenue of the whole hybrid power plant. An example of this dashboard is presented in Figure 19.

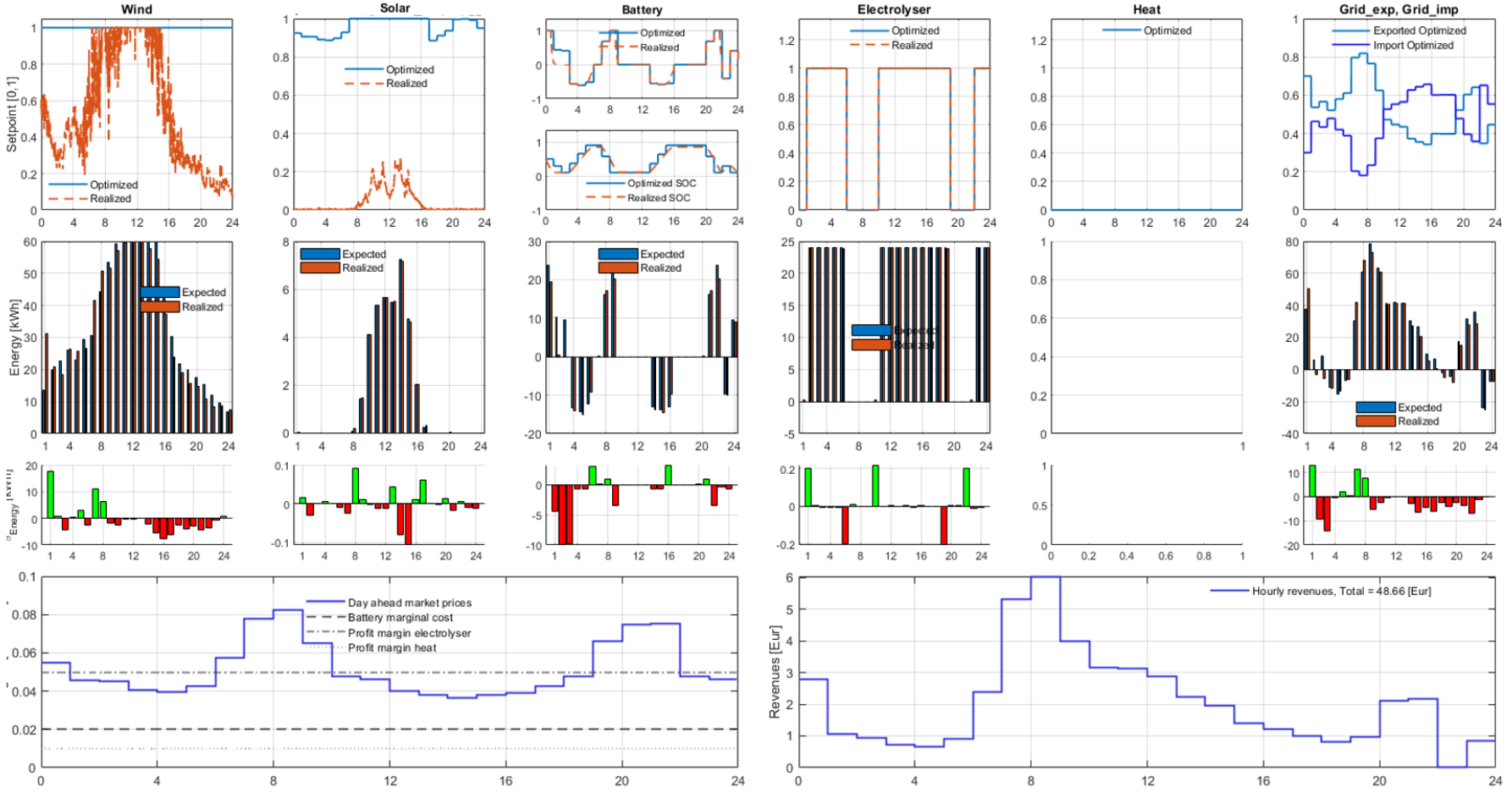

Figure 19: Final EMERGE dashboard with expected setpoints (top) and energy production (middle) for the day ahead at an hourly basis and actual realized from the 30 second based simulation, with differences between the expected and realized values shown (bottom). In addition, the market prices and relevant profit margins (bottom left) are shown, as are the realized revenues (bottom right).

4 Conclusion & recommendations

This work detailed the methodology behind the creation of TNO's Energy Management systEm for Renewable GeneratIon and storagE (EMERGE) model. This model was created in order to help answer technical and economic question around Hybrid Power Plants (HPPs). These HPPs are combined renewable generation, storage and conversion assets, operating as a single plant. In the EMERGE model, wind and solar photovoltaic (PV) generation can be simulated, combined with battery storage and hydrogen and heat conversion. In addition, an exemplifying case study was presented, to show the functionality of the EMERGE model.

Further recommendations for future work on the model include improvements to the individual assets, not only with more functionality but also fixing unresolved issues, such as the solar PV temperature increase from negative irradiance. Furthermore, expansion with revenue stacking options for HPP developers and subsequent connection to different electricity markets should be part of the future EMERGE functionality. The uncertainties that are related to these multiple market connections and the predictions that are required to bid on and participate in them, should also be part of this expansion. Finally, in order to consider using EMERGE for full-scale application, it should be experimentally validated first.

5 Bibliography

[1] Vladimir Lazarov et al. “Hybrid Power Systems with Renewable Energy Sources – Types, Structures, Trends for Research and Development.” In: Sept. 2005.

[2] Lennart Petersen et al. “Vestas Power Plant Solutions Integrating Wind, Solar PV and Energy Storage.” In: May 2018.

[3] TNO. *Keeping the electricity grid stable when there is a surplus of wind and solar*. URL: https://www.tno.nl/en/focus-areas/energy-transition/roadmaps/system-transition/towards-a-reliable-affordable-and-fair-energy-system/robustness-and-flexibility-of-the-energy-system/keeping-the-electricity-grid-stable-when-there-s-a-surplus-of-wind-and-solar/. (accessed: 04.06.2021).

[4] “Energy management strategies in hybrid renewable energy systems: A review.” In: *Renewable and Sustainable Energy Reviews* 62 (2016), pp. 821–835. ISSN: 1364-0321. DOI: https://doi.org/10.1016/j.rser.2016.05.040.

[5] Yimy E. García Vera, Rodolfo Dufo-López, and José L. Bernal-Agustín. “Energy Management in Microgrids with Renewable Energy Sources: A Literature Review.” In: *Applied Sciences* 9.18 (2019). ISSN: 2076-3417. URL: https://www.mdpi.com/2076-3417/9/18/3854.

[6] Juan P. Torreglosa et al. “Control based on techno-economic optimization of renewable hybrid energy system for stand-alone applications.” In: *Expert Systems with Applications* 51 (2016), pp. 59–75. ISSN: 0957-4174. DOI: https://doi.org/10.1016/j.eswa.2015.12.038. URL: https://www.sciencedirect.com/science/article/pii/S0957417415008465.

[7] Thomas Bak et al. “Baseline layout and design of a 0.8 GW reference wind farm in the North Sea.” In: *Wind Energy* 20 (9 2017), pp. 1665–1683. DOI: https://doi.org/10.1002/we.2116.

[8] Christian Bak et al. *Description of the DTU 10 MW Reference Wind Turbine*. Tech. rep. DTU Wind Energy Report-I-0092. DTU Wind Energy, June 2013. URL: http://orbit.dtu.dk/files/55645274/The_DTU_10MW_Reference_Turbine_Christian_Bak.pdf.

[9] P.M.O. Gebraad et al. “Wind plant power optimization through yaw control using a parametric model for wake effects - a CFD simulation study.” In: *Wind Energy* 19(1) (2014), pp. 95–114.

[10] Marcelo Gradella Villalva, Jonas Rafael Gazoli, and Ernesto Ruppert Filho. “Comprehensive Approach to Modeling and Simulation of Photovoltaic Arrays.” In: *IEEE Transactions on Power Electronics* 24.5 (2009), pp. 1198–1208. DOI: 10.1109/TPEL.2009.2013862.

[11] Vinod, Raj Kumar, and S.K. Singh. “Solar photovoltaic modeling and simulation: As a renewable energy solution.” In: *Energy Reports* 4 (2018), pp. 701–712. ISSN: 2352-4847. DOI: https://doi.org/10.1016/j.egyr.2018.09.008. URL: https://www.sciencedirect.com/science/article/pii/S2352484718300842.

[12] *Modeling and Analysis of a Battery Energy System Supplied from Photovoltaic Power Source*. June 19-20 2014.

[13] H.L. Chan. “A new battery model for use with battery energy storage systems and electric vehicles power systems.” In: *2000 IEEE Power Engineering Society Winter Meeting. Conference Proceedings (Cat. No.00CH37077)*. Vol. 1. 2000, 470–475 vol.1. DOI: 10.1109/PESW.2000.850009.

[14] *”E4tech element energy: Appendixes - Electrolysis in the EU”*. Tech. rep.

[15] M. Kopp et al. “Energiepark Mainz: Technical and economic analysis of the worldwide largest Power-to-Gas plant with PEM electrolysis.” In: *International Journal of Hydrogen Energy* 42.19 (2017). Special Issue on The 21st World Hydrogen Energy Conference (WHEC 2016), 13-16 June 2016, Zaragoza, Spain, pp. 13311–13320. ISSN: 0360-3199. DOI: https://doi.org/10.1016/j.ijhydene.2016.12.145. URL: https://www.sciencedirect.com/science/article/pii/S0360319917300083.

[16] Andreas Bloess, Wolf-Peter Schill, and Alexander Zerrahn. “Power-to-heat for renewable energy integration: A review of technologies, modeling approaches, and flexibility potentials.” In: *Applied Energy* 212 (2018), pp. 1611–1626. ISSN: 0306-2619. DOI: https://doi.org/10.1016/j.apenergy.2017.12.073. URL: https://www.sciencedirect.com/science/article/pii/S0306261917317889.

[17] T. Ding et al. “Big-M Based MIQP Method for Economic Dispatch With Disjoint Prohibited Zones.” In: *IEEE Transactions on Power Systems* 29.2 (Mar. 2014), pp. 976–977. ISSN: 0885-8950. DOI: 10.1109/TPWRS.2013.2287993.

[18] Michael Schimpe et al. “Marginal Costs of Battery System Operation in Energy Arbitrage Based on Energy Losses and Cell Degradation.” In: *2018 IEEE International Conference on Environment and Electrical Engineering and 2018 IEEE Industrial and Commercial Power Systems Europe (EEEIC / I CPS Europe)*. 2018, pp. 1–5. DOI: 10.1109/EEEIC.2018.8493717.

[19] International Energy Agency (IEA). *The Future of Hydrogen: Seizing today’s opportunities*. https://www.iea.org/reports/the-future-of-hydrogen. Accessed: 2021-12-17.

[20] KPMG. *The hydrogen trajectory: What does research tell us about the pace of development of hydrogen technologies*. https://home.kpmg/xx/en/home/insights/2020/11/the-hydrogen-trajectory.html. Accessed: 2021-12-17.

[21] *Measurement and Insrumentation Data Center (MIDC)*. https://midcdmz.nrel.gov/. Accessed: 2021-12-17.

[22] Amit Jain and Avinashi Kapoor. “Exact analytical solutions of the parameters of real solar cells using Lambert W-function.” In: *Solar Energy Materials and Solar Cells* 81.2 (2004), pp. 269–277. ISSN: 0927-0248. DOI: https://doi.org/10.1016/j.solmat.2003.11.018. URL: https://www.sciencedirect.com/science/article/pii/S0927024803002605.

[23] Clifford Hansen. *Parameter Estimation for Single Diode Models of Photovoltaic Modules*. Tech. rep. Mar. 2015.

[24] “A detailed modeling method for photovoltaic cells.” In: *Energy* 32.9 (2007), pp. 1724–1730. ISSN: 0360-5442. DOI: https://doi.org/10.1016/j.energy.2006.12.006. URL: https://www.sciencedirect.com/science/article/pii/S0360544206003501.

[25] “Determining the optimum grid-connected photovoltaic inverter size.” In: *Solar Energy* 87 (2013), pp. 96–116. ISSN: 0038-092X.

[26] Giuliano Rancilio et al. “Modeling a Large-Scale Battery Energy Storage System for Power Grid Application Analysis.” In: *Energies* 12.17 (2019). ISSN: 1996-1073. URL: https://www.mdpi.com/1996-1073/12/17/3312.

[27] Olivier Tremblay, Louis-A. Dessaint, and Abdel-Illah Dekkiche. “A Generic Battery Model for the Dynamic Simulation of Hybrid Electric Vehicles.” In: *2007 IEEE Vehicle Power and Propulsion Conference*. 2007, pp. 284–289. DOI: 10.1109/VPPC.2007.4544139.

[28] Håvard Breisnes Vika. “Modelling of Photovoltaic Modules with Battery Energy Storage in Simulink/Matlab | With in-situ measurement comparisons.” MA thesis. Nowergian University of Science and Technology, Department of Electric Power Engineering, June 2014.

[29] Weixiang Shen, Thanh Tu Vo, and Ajay Kapoor. “Charging algorithms of lithium-ion batteries: An overview.” In: *2012 7th IEEE Conference on Industrial Electronics and Applications (ICIEA)*. 2012, pp. 1567–1572. DOI: 10.1109/ICIEA.2012.6360973.

[30] Pierre Olivier, Cyril Bourasseau, and Belkacem Bouamama. “Dynamic and multiphysic PEM electrolysis system modelling: A bond graph approach.” In: *International Journal of Hydrogen Energy* 42.22 (2017), pp. 14872–14904. ISSN: 0360-3199. DOI: https://doi.org/10.1016/j.ijhydene.2017.03.002. URL: https://www.sciencedirect.com/science/article/pii/S036031991730839X.

[31] Petronilla Fragiacomo and Matteo Genovese. “Modeling and energy demand analysis of a scalable green hydrogen production system.” In: *International Journal of Hydrogen Energy* 44 (Oct. 2019). DOI: 10.1016/j.ijhydene.2019.09.186.

[32] Maja Persson, Dimitri Mignard, and David Hogg. “Insights on performance and an improved model for full scale electrolysers based on plant data for design and operation of hydrogen production.” In: *International Journal of Hydrogen Energy* 45 (Nov. 2020), pp. 31396–31409. DOI: 10.1016/j.ijhydene.2020.08.255.

[33] Julio José Caparrós Mancera et al. “An Optimized Balance of Plant for a Medium-Size PEM Electrolyzer: Design, Control and Physical Implementation.” In: *Electronics* 9.5 (2020). ISSN: 2079-9292. URL: https://www.mdpi.com/2079-9292/9/5/871.

A Detailed modelling approach

A.1 Wind Farm model

The wake simulation model used in this work is based on the FLORIS wind farm model [9]. The model is widely used by the wind farm control community due to its simplicity and fast calculation speed, making is very suitable for use in optimization algorithms such as the EMS considered here. The Matlab implementation of the FLORIS code has been used here, which is freely available through the TU-Delft GitHub repository https://github.com/TUDelft-DataDrivenControl/FLORISSE_M. The FLORIS model settings used in this study are listed in Table 2, while the model parameters have been left unchanged. As the HyPP model has been developed in Simulink, and the original Matlab implementation of FLORIS was not runnable directly from Simulink, large part of the model has been modified to enable usage in Simulink. No functional modifications have been done, though, and the modified code has been verified against the original version to produce equivalent results. Even though the model is stationary, it is considered suitable enough for performing quasi-dynamic simulations for the purpose of design and analysis of the EMS with the main focus on participation in the day-ahead or intra-day energy markets, which operate at hourly to quarter of an hourly basis. Nevertheless, the HyPP simulation model allows also faster simulations, e.g. at 30 seconds to 1 minute sample times, to simulate the actual power production with reasonable variations in the actual power production. This enables evaluation of the power imbalance, and makes it possible to include uncertainty into the modelling for future studies.

Table 2: FLORIS model settings and parameters used in the study

FLORIS parameter	Value
Atmospheric inflow	Uniform
Wake deficit model	Porté-Agel
Wake deflection model	Porté-Agel
Wake mixing model	Katic
Turbine-induced turbulence model	Porté-Agel

The wind farm model used in this study is the Norcowe reference wind farm, in its regular baseline case as described in [7]. The wind farm consists of 80 wind turbines of the DTU 10 MW reference wind turbine [8]. In FLORIS, the wind turbines are modelled through their aerodynamic power and thrust coefficients, expressed as function of the pitch angle and the wind velocity. The turbine model has been extended here with a simple wind turbine control logic that regulates the wind turbine's power production to track the power production set-point coming from the EMS. More specifically, the turbine controller implements delta power control by accepting a relative power production set-point, treated as percentage of the available power (e.g. 80% of available power), and modifies the pitch angle to ensure that the power production is curtailed in accordance with the set-point. The turbine controller also provides an estimate of the available power production to the EMS. The FLORIS model is driven by ambient wind conditions (wind direction, wind speed and turbulence intensity), which are uniform over the whole farm but vary in time.

A.2 The solar PV model

The solar farm model is based on the modelling of the individual solar panels. Each solar panel is modelled by using its electrical circuit equivalent representation. Such representation can have a lower or higher level of accuracy, depending on the parameters that are taken into consideration.

In Figures 20,21 and 22 the three most common equivalent citcuit models used to simulate the behaviour of a solar panel are represented. From left to right, they are order by their level of complexity.

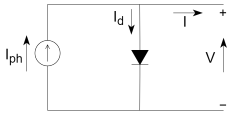

Figure 20: Simplified equivalent circuit of an ideal PV solar cell using the single diode model.

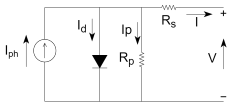

Figure 21: Equivalent circuit of a real model for a PV panel using the single diode model.

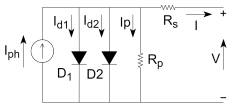

Figure 22: Equivalent circuit model of a real PV cell using the double diode model.

For the purposes of this work, the model in Figure 21 is chosen, as it is a good balance between accuracy and complexity. The underlying equations are used to build the I-V and P-V curves of the solar panel [10, 11, 12]. The final equation is transcendental in nature, i.e., it is not possible to solve the current-voltage relationship explicitly for one of the variables. To overcome this, the Lambert-$\mathcal{W}$ function solution is used, i.e, an exact closed-form solution based on the latter function is employed to express the current as an explicit analytical function of the terminal voltage [22, 23]. With this formulation, the existence of a Maximum Power Point Tracking (MPPT) controller is assumed, i.e, at each time instant k, given the existing atmospheric conditions (temperature, irradiance), the power production of the solar panel is assumed to be maximum by manually selecting the maximum point in the P-V curve.

The output current of the solar cell can be written by making use of Kirchoff's first law, as described in equation A.1.

$$I = I_{ph} - I_d - I_p \tag{A.1}$$

where I_{ph} is the current generated by the incident light (hence directly proportional to the sun irradiation), I_d is the internal diode current given by the Schockley diode current equation and I_p is the shunt current across the p-n junction. The series resistance R_s and parallel resistance R_p in Figure 21 model the efficiency of the solar cell. R_s incorporates the losses by Joule effect, primarily due to metal grids, semiconductor materials, collecting bus and its connections [11]. R_p is associated with seepage effects of current [11, 10]. The values for the resistances have to be estimated based on experimental data of the solar cell. The effects of the resistances can be neglected by setting R_s to very low values and R_p to high values, winch boils down to using the model in Figure 20.

The terms in equation A.1 can be written more explicitly, as shown in equation A.2.

$$I = \underbrace{\left[I_{sc} + K_i(T_o - T_r)\right]\frac{G}{G_{ref}}}_{I_{ph}} - \underbrace{I_o\left[\exp\left(\frac{V + IR_s}{nV_{th}}\right) - 1\right]}_{I_d} - \underbrace{\frac{V + IR_s}{R_p}}_{I_p} \tag{A.2}$$

The generated photo current I_{ph} depends linearly on the solar irradiation G [W/m^2]. G_{ref} is the irradiance at nominal conditions, 1000 W/m^2. T_o is the temperature at

nominal conditions (25°C) and T_r the actual temperature, both in Kelvin degrees. I_{sc} [A] is the short-circuit current, i.e., the maximum current available at the terminals of the device and K_i [%/°C] is the cell short circuit current temperature coefficient.

The diode current I_d is known from the theory of semiconductors [11]. The diode ideality factor is represented by n (unitless). The termed V_{th} is termed the thermal voltage (V) of the module, which is determined from the cell temperature T_r, Boltzmann's constant k [J/K] and the elementary charge [Couloumb] and the number of identical cells in series, N_S, $V_{th} = N_s k T_c/q$ [23]. I_o is the saturation current of the diode, and its full computation is seen in equation A.3.

The term I_{rs} refers to the reverse saturation current, which is computed using equation A.4. E_g [eV] is the energy band gap, dependent on the solar cell module, and V_{oc} corresponds to the open circuit voltage.

$$I_o = I_{rs}\left[\frac{T_o}{T_r}\right]^3 \exp\left[\left(\frac{qEg}{nK}\right)\left(\frac{1}{T_r}-\frac{1}{T_o}\right)\right] \tag{A.3}$$

$$I_{rs} = \frac{I_{sc}}{\exp\left(\frac{qV_{oc}}{N_s K n T_o}\right)-1} \tag{A.4}$$

To simulate the power production of the solar cell it is necessary to know the temperature of the photovoltaic module. This can be modelled as a function of ambient temperature, wind speed and total irradiance [24], as stated in equation A.5.

$$T_r(^\circ C) = 0.943 T_a + 0.028 G - 1.528 v + 4.3 \tag{A.5}$$

where T_a is the ambient temperature in °C and v the wind speed [m/s].

The transcendental nature of the I-V equation is clear from equation A.2, where the output current I on the left side of the equation depends on the exponential of its value on the right side. To overcome this, the current is expressed as a function of voltage $I = I(V)$, by using the transcendental Lambert's $\mathcal{W}$ function. The later function is the solution of the equation $x = \mathcal{W}\exp[\mathcal{W}(x)]$, as fully detailed in [22, 23]. Using this function, the solution is written in equation A.6.

$$\begin{aligned} I =& \frac{R_p}{R_p+R_s}(I_{ph}+I_o) - \frac{V}{R_p+R_s} \\ & - \frac{nV_{th}}{R_s}\mathcal{W}\left(\frac{R_p I_o}{nV_{th}}\frac{R_p}{R_p+R_s}\exp\left(\frac{R_p}{R_p+R_s}\frac{R_p(I_{ph}+I_o)+V}{nV_{th}}\right)\right) \end{aligned} \tag{A.6}$$

By combining equations A.1, A.2, A.3, A.4, A.5 and the explicit solution in A.6, for the given atmospheric conditions (irradiance and atmospheric temperature) the I-V and P-V curves can be computed and the power output of the solar cell is known.

The values used for the solar panel are based on the model KC200GT specified in [10]. All the values are listed in Table 3.

Table 3: Parameters of the KC200GT Solar Array

Type	Variable	Description	Unit	Value
Eletrical and physical constants	q	Electron charge	coloumb	$1.6021*10^{-19}$
	K	Boltzmann constant	J/K	$1.3806*10^{-23}$
	Eg	Band gap energy of semiconductor	eV	1.12
Manufacturer specified	I_{sc}	Short circuit current	A	8.21
	V_{oc}	Open circuit voltage	V	32.9
	k_i	Cell short circuit current temperature coefficient of I_{sc}	A/K	0.0032
	A	Diode ideality factor	-	1.3
Configuration	Ns	Total series cells	#	54
	Np	Total parallel cells	#	1
Reference values	T_0	Reference temperature	°C	25
	G_{ref}	Refernce irradiance	W/m^2	1000
Estimated	Rs	Series resistance	Ohm	0.221
	Rp	Parallel resistance	Ohm	415.405

The aforementioned equations were implemented in a MATLAB block function in Simulink, where the output, at each time instant k, is the P-V curve for the given ambient conditions. The maximum value of this array is then chosen and the output of the solar panel is normalized with relation to is maximum power production, 200 W. The inverter connected to the grid is undersized to approximately 90%, i.e., the minimum value between the undersizing ratio and normalized production is the effective output of the single solar panel. This is a common procedure since the high-in plane irradiance does not occur often and the temperature effects make it difficult of achieving rated power, and hence a trade-off between energy yield maximisation and invert cost minimisation should be made [25].

A.3 Battery Energy Storage model

Different approaches exist in order to model the behaviour of a Battery Energy Storage System (BESS), depending on the model's application. This may range from eletrochemical models which are focused on the reactions occuring in each cell, attempting to precisely model the nature of the battery, to equivalent circuit models. The former feature extreme high computational accuracy, accompanied by a large effort. The latter, on the other hand, offers a better compromise between accuracy and computational time [26].

For the purposes of this work, an equivalent circuit model is employed, in order to reduce the required computational effort with acceptable accuracy. In this case, a typical battery circuit model was adapted from literature [13], representing the battery cell as a controlled voltage source and a constant series internal resistance, as shown graphically in Figure 23.

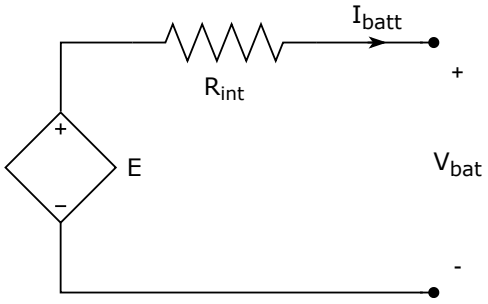

Figure 23: Equivalent circuit model of a simplified battery cell using a controlled voltage source and constant series internal resistance. Adapted from [13].

The calculation of the no-load voltage E of the battery is again adapted from literature [27, 28], and defined in Equation A.7.

$$E = E_0 - K\frac{Q_0}{Q} + A \cdot e^{-B(Q_0 - Q)} \tag{A.7}$$

Here, E_0 is the battery constant voltage, K is the polarisation voltage, Q_0 is the rated battery capacity [Ah], Q is the current battery capacity [Ah], A is the exponential zone amplitude [V] and B is the exponential zone time constant inverse [Ah^{-1}]. The current battery capacity Q and battery voltage V_{bat} are unchanged from literature, and calculated as shown in Equation A.8 and Equation A.9.The parameters used for the battery, which is assumed to be a lithium-ion cell, are shown in Table 4. These parameters are again based on literature, chosen in such a way that the charging and discharging curves are in line with empirical results from physical cells [27, 28].

Table 4: Parameters of the lithium-ion cell used in the model [27]

Parameters	Lithium-ion cell (1 Ah)
E_0 [V]	3.7348
R_{int} [Ω]	0.09
K [V]	0.00876
A [V]	0.468
B [Ah^{-1}]	3.5294

$$Q = Q_{start} + \int_0^t -I_{batt}\, dt \tag{A.8}$$

$$V_{bat} = E - I_{batt} \cdot R_{int} \tag{A.9}$$

The controller or battery management system (BMS) of the battery is used to limit the state-of-charge and ingoing and outgoing current of the battery. This is handled by first calculating the required current and then voltage based on the requested setpoint, as shown in Equation A.10 and A.11. Here, I_{sp} is the current setpoint, SP is the requested setpoint (between -1 and 1), I_{max} is the maximum charging/discharging current, V_{sp} is the voltage setpoint and V_{int} is the internal voltage of the battery. Finally, the new state of charge (SOC) is calculated in A.12.

$$I_{sp} = SP \cdot I_{max} \tag{A.10}$$

$$V_{sp} = V_{int} - I_{sp} \cdot R_{int} \tag{A.11}$$

$$SOC = \frac{Q}{Q_0} \tag{A.12}$$

These equations are implemented as a MATLAB block function in Simulink, the new state of charge (SOC) is then calculated by determining E using equation A.7, which in turn is used to calculate I_{batt} using equation A.9. Following this, the new battery capacity Q is calculated using equation A.8. Finally, the battery SOC is determined using equation A.12.

In addition to determining the SOC, the BMS is also tasked with protecting against over- and undercharging of the battery. In practice, this means the BMS is implemented

to ensure that $SOC_{min} \leq SOC \leq SOC_{max}$. Furthermore, a typical way of charging Li-ion batteries is using constant current, constant voltage (CC-CV), which leads to slower charging in the high SOC regions of the battery. On top of this behaviour, the BMS can limit power in low SOC regions, due to strongly decreasing voltage [29]. To emulate these behaviours, the maximum current is calculated to be linearly decreasing below and above a SOC threshold SOC_{low} and SOC_{high}, respectively.

A.4 Electrolyser

Several electrolyser models exist in literature which reflect the electrochemical operation happening at the stack. Most models consider mainly the stack rather than the whole system in which other physical parameters and domains govern the dynamics (e.g. heat dissipation constraints, controller functions). One of the most detailed modelling approach is the generic multi-physics dynamical model using Bond Graph approach as used in [30]. This approach takes into account all physical domains and links them with a Bond Graph technique. This model is suitable for modelling, control, sizing and diagnosis analysis of PEM electrolysis systems. It might however be too detailed for the purpose of the Energy Management System (EMS). Another modelling technique is to use mathematical models to represent the energy flows, auxiliaries, electricity and heat occurring in all subsystems as presented in [31].

All these modelling techniques are quite detailed in terms of physical modelling but lack the realistic representation of states that an electrolyser would operate. Therefore, in the current article, the electrolyser system (stack + Balance Of Plant (BOP)) is modelled with an operational status-based static model with efficiency look-up tables taking into account electrolyser stack and BOP power consumption and ramp rates. The electrolyser stack and BOP power consumptions come from specific literature and characteristic curves, while the ramp rates are based on what is available currently in theoretical and experimental literature ranging from kilowatt (kW) applications up to megawatt (MW) applications. In terms of a practical implementation, this straightforward and rather concise approach is configured inside a Simulink block.

The electrolyser receives normalized power consumption loading set-points ([0,1]) from the optimization algorithm that schedules the entire HyPP. Therefore, the electrolyser will aim to reach this set-point but always respecting the technical limitations and restrictions expressed in ramp rates or timer functions. The output of the electrolyser model is the realized hydrogen production rate [kg/s] within the specified time integration or sampling time of the simulation. Figure 24 below indicates the system power consumption curves for the hydrogen production and are adapted from a 250kW electrolyser study in [32] and power consumption information in [14] corrected by adding the lower heating value (LHV) of hydrogen to all system inefficiencies. The left plot in Figure 24 shows the electrical consumption per kgH_2 produced for each normalized set-point, while the right one shows the total hydrogen production per hour for a 24kW electrolyser system example.

The model is based on 3 states of operation for which different ramp rates are assigned in order to approximate the time to reach a set-point. If the theoretical ramp rate needed to reach a set-point is simply to fast then the system will respect its technical constraints of the ramp-rates relevant at each state. The system is assumed to reach operational state whenever a set-point is reached. Each state has a timer variable which accounts for changing from a specific state to another:

1. *The first state is the off-state*: is when the electrolyser is turned-off. The electrolyser can come to an off-state from the cold-standby state (explained in the second). If a set-point is given for the electrolyser to produce a certain amount of hydrogen or consume a certain amount of power, then a particular

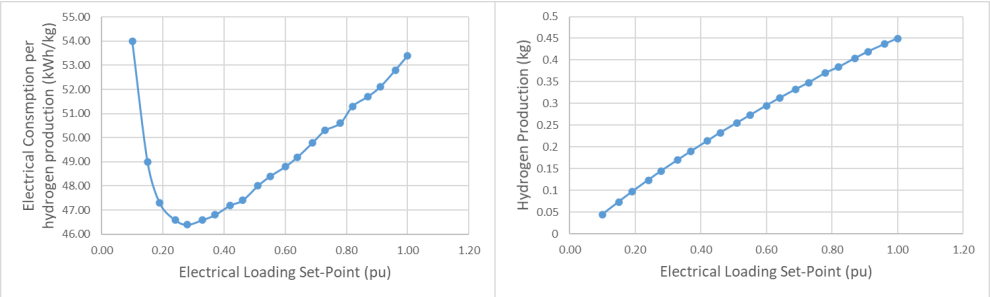

Figure 24: Input-output variables of electrolyser model. Adapted from 250kW electrolyser study [32] and power consumption information in [14]. On the left plot the electrical consumption per kgH2 and on the right plot the total hourly production for a 24kW electrolyser system example.

ramp-rate is respected from the off-state up to production which takes about 840 seconds, a duration assumed from a kW-scale electrolyser reference in [33]. This duration includes all necessary processes (e.g. purging, heating up, increase of pressure) in order to reach a fully functional operational state (third and last stage explained in the third point). Therefore the ramp rate to be operational is 1/840=0.0011 $\frac{pu}{second}$.

2. *The second state is the cold standby*: is a state when the electrolyser enters if it has not received a production set-point for 180 seconds, measured with a timer function in the model. Therefore, a cold standby comes only from an operational state, explained later. If the electrolyser when in cold-standby receives a set point then the ramp rates differ from the ones in the operational state as the balance-of-plant needs to readjust some electrochemical, thermal (water and stack temperature) and fluid parameters (pressures). Therefore, there are some slower dynamics until the system returns to operational state again. The ramp rates are 0.011 pu/second (both ramp-up and ramp-down), values assumed from the following kw and MW scale electrolyser research projects in [14], [15]. If the electrolyser, during cold-standby, stays for longer than 300 seconds then it enters the Off-State, explained above.

3. *The third state is the operational state*: is when the electrolyser is producing hydrogen or is in hot-standby (having not received any setpoint larger than 0% for a maximum duration of 300 seconds after a hydrogen producing state). The ramp rates valid for this state are 0.1 pu/s (ramp-up) and 0.2 pu/s (ramp-down), which are based on the following kW and MW scale electrolyser demonstrations in [14], [15]. A timer function that brings the electrolyser to cold standby is set to 300 seconds, as explained as well above.

A.5 Heat Pump

For the power to heat asset, a heat pump is modelled based on known equations from thermodynamics which govern its behaviour, based on the overview of different modelling approaches in [16]. For a heat pump, an accurate relation between the heat output $\dot{Q}$ and the power input P_{hp} needs to be defined to accurately capture the behaviour of the heat pump. Such relation is accomplished with the Coeficient of Performance (COP), which relates the useful heating provided to energy required.

In the modelling approach taken, a varying COP is used, as in reality the latter ratio depends on the temperature levels of the energy source T_{source} and sink T_{sink}, as expressed by the Carnot-COP COP_{carnot} [16].

$$COP_{Carnot} = \frac{T_{sink}}{T_{sink} - T_{source}} \tag{A.13}$$

For the purposes of this work, T_{source} corresponds to the temperature of the environmental air used to provide heat to greenhouses and T_{sink} is then the desired temperature the greenhouse should be maitained. A quality grade ϕ to account for technical progress is introduced, i.e., the ratio between achieveable COP and the theoretically achievable one for the given temperature conditions [16].

$$\phi = \frac{COP_{real}}{COP_{carnot}} \tag{A.14}$$

The equation relating the heat output provided by the heat pump and the eletrical input power follows in A.15:

$$P_{hp} = \frac{\dot{Q}}{COP_{real}} = \frac{\dot{Q}}{\phi \frac{T_{sink}}{T_{sink} - T_{source}}} \tag{A.15}$$

This formualtion representes only an approximation, as in reality T_{sink} is affected by the output $\dot{Q}$. However modelling the later dependence would yield a non linearity and increase computational effort, which is not desirable. [16]

A.6 Electrical Network

The simulation model of the electrical parts of the hybrid power plant used in this work consists of:

a. *Grid coupling through power-electronic converters*

Each of the power generation, conversion and storage systems is coupled to the internal low-voltage (Alternating Current) AC-grid through a power-electronic converter. Each converter can either supply power to or withdraw power from the grid, which is determined by its setpoint, operational conditions and limitations. The model is highly simplified[1], i.e. stationary and lossless, in order not to slow down the simulation. Like all other electrical models in this simulation the converters assume only symmetrical and fundamental (i.e. 50Hz.) voltages and currents.

- Each converter receives an active power P [W] and reactive power Q [VAr] setpoint, which is normalised to the rated power S_{rated} [VA] of the respective subsystem (e.g. the individual PV-array or wind turbine), so between -1.0 and 1.0 [-]. Depending on the reactive power mode parameter (as defined in the initial electrical system configuration), the reactive power output can also be set to zero or to a constant Power Factor (PF):

$$PF = \frac{P}{\sqrt{P^2 + Q^2}}. \tag{A.16}$$

- The output power of each converter is instantly limited in case its maximum output current is reached. The voltage at each converter AC-terminal is used as input in order to respond to grid voltage dips, i.e. by limiting the

[1] [note: KIP2020 simulation models also included converter averaged, positive-sequence dynamics]

output power. The power limitation method is a proportional reduction of both the active and reactive power (i.e. with equal priority to active and reactive power). If needed, prioritization of reactive power provision (instead of proportional power limitation) during to voltage dips can easily be implemented in future versions.

- The converter outputs power levels are given in per-unit values [p.u.], with 100kW as the per-unit base power, as being the approximate maximum power production of the modelled power plant) in order to generalize the network calculations. For example, P_{pu}= 0.8 [p.u.], Q_{pu} = 0.05 [p.u] equals P = 80kW, Q = 5kVAr.
- Finally, the grid coupling model includes the network topology, as defined in the initial electrical system configuration, to link the converters to the respective systems (e.g. PV arrays, wind turbines) and network nodes.

b. *Load flow calculation of the local low-voltage electric grid*

The electrical grid model includes lumped impedance models of all cable connections in the local AC-grid. The single connection to the utility grid is simply modelled as an infinite slack bus at a fixed voltage of 1.0 [p.u.]. All voltages, currents are represented as complex numbers in the per-unit system, based on S_{base} = 100kVA and V_{base} = 400V.

Three calculations are performed for this network: (1) The load flow is calculated through an iterative approximation; (2) the resulting network losses are calculated; (3) any overload of cables is determined (only assuming excess power input to the network) and reduced power setpoints for the next iteration are calculated. The overload algorithm first sorts the cables, starting with the most heavily (relative) overloaded cable. For any overloaded cable, say between node a and b, with the power flowing from a to b, the required reduction of power at node a is approximated.

c. *Grid overload limitation by setpoint adaptation*

As a next step, the required power generation reduction or load increase per network node is dispatched between the different assets. This is done according to the following priorities: 1) increase electrolyzer production setpoint, 2) increase charging or decrease discharging setpoint of battery, 3) curtail PV array, 4) curtail wind turbines. The update frequency of these network calculations is set to 1 second.